VII International Conference on Computational Methods for Coupled Problems in Science and Engineering
COUPLED PROBLEMS 2017
M. Papadrakakis, E. Oñate and B. Schrefler (Eds)

FLUID–STRUCTURE INTERACTION DESIGN OF INSECT–LIKE MICRO FLAPPING WING

D. ISHIHARA*, N. OHIRA*, M. TAKAGI*, S. MURAKAMI* AND T. HORIE*

* Department of Mechanical Systems Engineering
Kyushu Institute of Technology
680-4 Kawazu, Iizuka, Fukuoka 820-8502, Japan
e-mail: ishihara@mse.kyutech.ac.jp, www-solid.mse.kyutech.ac.jp

Key words: Fluid–Structure Interaction, Insect Flapping Flight, Micro–Electro–Mechanical Systems, 2.5–Dimensional Structure, Micro Air Vehicle, Projection Method, Design Window.

Abstract. In this study, a FSI design of an insect–like micro flapping wing is proposed. Similar to actual insects, the proposed design actively uses the FSI to create the passive wing motions. Each design solution has a 2.5–D structure for the MEMS technology. The 3–D unsteady monolithic FSI equation system is solved to find the satisfactory design solutions using a projection method in a parallel computation environment. An area of satisfactory design solutions in a design parameter space or Design Window (DW) is presented. Each design solution in the present DW can generate the thrust sufficient to support the weight of the model insect. Therefore, the insect–like MEMS–based MAVs are possible.

1 INTRODUCTION

In this study, a FSI design of an insect–like micro flapping wing is proposed. Similar to actual insects, the proposed design actively uses the FSI to create the pitching motion of the wing. The proposed design will decrease the mechanical complexity of MAVs. The proposed design requires the accurate and stable analysis for the strong interaction. Furthermore, the speedup of computation is required for the parametric study. Therefore, a projection method using the algebraic splitting [1, 2] is used to solve the 3–D unsteady monolithic FSI equation system in a parallel computation environment.

Each design solution has a 2.5–D structure for the MEMS processing. The initial design parameters are determined based on a model insect. An area of satisfactory design solutions in a design parameter space or Design Window (DW) is presented. DW is convenient for decision-making in MEMS structural design [3]. Each solution in the present DW can generate the thrust sufficient to support the weight of the model insect. These results show the possibility of insect–like MEMS–based MAVs. It follows from the present results that the artificial micro system mimicking the organisms can use the coupled problem to create its function, and the 2.5–D structure can be designed with the aid of recent progress in coupled analysis [4, 5] such that it can be fabricated using the MEMS technology.

2 FLUID–STRUCTURE INTERACTION DESIGN

2.1 Concept

Fig. 1 shows the conceptual view of the insect–like MEMS–based MAV, where the insect flapping flight mechanics and the MEMS technology are combined. Following actual insets, the insect–like MAV can be minimized from 1mm to 1cm in size. At these size scales, the MEMS technology would be most promising. The FSI design is proposed to develop it.

The main design concept is the active use of the FSI to create the function in micro system: Similar to actual insects, an insect–like micro flapping wing actively uses the FSI to create the pitching motion. It will decrease the mechanical complexity of MAVs. Furthermore, the 2.5–D structure is used such that it can be fabricated using the MEMS technology.

2.2 FSI cause of pitching motion

The wing motion consists of the flapping and the pitching as shown in Fig. 2. The interaction between the flapping flexible wing and the surrounding air can create the characteristic pitching motion and the enough lift for the insect to hover [6–9].

2.3 Insect–like micro flapping wing

Fig. 3 shows the schematics of the insect–like micro flapping wing based on the proposed FSI design. As shown in this figure, the 2.5–structure is adopted: The flexible wing is fabricated using the membrane. The beam is used as the leading edge to support the wing membrane. Taking into account micro actuator, the plate spring at the base amplifies the stroke angle using the resonance.

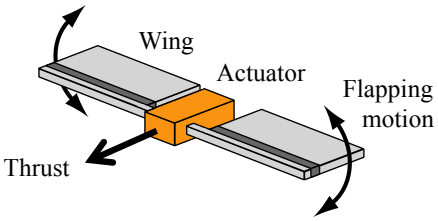

Figure 1: Insect–like MEMS–based MAV.

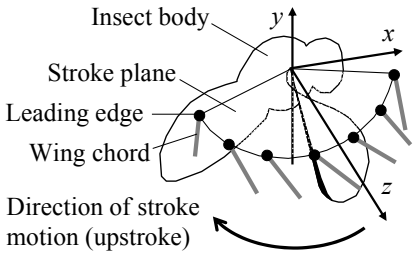

Figure 2: Schematics of insect flapping flight.

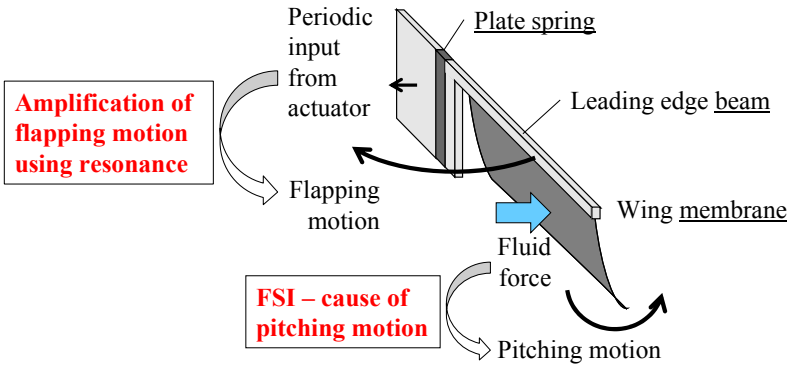

Figure 3: Schematics of the insect–like micro flapping wing based on the proposed FSI design.

3 FLUID–STRUCTURE INTERACTION ANALYSIS

3.1 Governing equations for FSI

The equilibrium equation for the elastic body and the incompressible Navier–Stokes equations are considered to describe the motion of the deformable model wing and the fluid flow surrounding the wing, respectively. The arbitrary Lagrangian–Eulerian method is used to describe the motion of the fluid–structure interface. The interface conditions to describe the interaction between the wing and the surrounding fluid are considered.

3.2 Monolithic equation system for FSI

Applying finite element discretization to the total Lagrangian formulation of the equation of the elastic body, the nonlinear equilibrium equation system can be obtained in matrix form. Similarly, the nonlinear equation system of the incompressible viscous fluid can be obtained in matrix form. Applying the interface conditions to these spatially discretized governing equations, the monolithic equation system can be obtained as

$$ {}_{\mathrm{L}}\mathbf{Ma}+\mathbf{Cv}+\mathbf{N}+\mathbf{q}(\mathbf{u})-\mathbf{Gp}=\mathbf{g}\,,\ {}_{\tau}\mathbf{Gv}=\mathbf{0}\,, \qquad \text{(1a, b)} $$

where **M**, **C,** and **G** are the mass, diffusive, and divergence operator matrices, **N**, **q**, **g**, **a**, **v**, **u**, and **p** are the convective term, elastic internal force, external force, acceleration, velocity, displacement, and pressure vectors, respectively, the subscripts L and τ indicate the lumping of the matrix and the transpose of the matrix, respectively.

Eq. (1) is linearized using the state variable increments to obtain the following equations:

$$ \mathbf{M}^{*}\Delta\mathbf{a}-\mathbf{G}\Delta\mathbf{p}=\Delta\mathbf{g}\,,\ \gamma\Delta t\,{}_{\tau}\mathbf{G}\Delta\mathbf{a}+\mathbf{G}_{\varepsilon}\Delta\mathbf{p}=\Delta\mathbf{h}\,, \qquad \text{(2a, b)} $$

where the pressure and elastic interior force terms are evaluated implicitly, $\mathbf{M}^{*}$ is the generalized mass matrix, Δ denotes the increment, t denotes the current time, Δ**g** and Δ**h** are the residual vectors of Eq. (1), respectively, $\mathbf{G}_{\varepsilon}$ is come from the pressure stabilization [10], and the relations among the state variables are $\Delta\mathbf{u}=\beta\Delta t^{2}\Delta\mathbf{a}$ and $\Delta\mathbf{v}=\gamma\Delta t\Delta\mathbf{a}$ based on Newmark's method. The predictor–multicorrector algorithm is used for the time integration.

3.3 Projection method using algebraic splitting

The monolithic method solves Eq. (2) and satisfies the interface conditions to avoid spurious numerical power on the interface, which yields numerical instability. However, the formulation leads to an ill–conditioned equation system. Therefore, the projection method using the algebraic splitting [2] is used to avoid this difficulty. The present method was first proposed in [1], and modified in [2]. The present method is briefly described as follows:

The state variables is predicted as the intermediate state variables from Eq. (1a) for the known pressure, which is linearized as

$$ \mathbf{M}^{*}\Delta\hat{\mathbf{a}}=\Delta\mathbf{g}\,, \qquad (3) $$

where $\hat{\mathbf{a}}$ is the intermediate acceleration. Subtracting both sides of (3) from (2a) gives,

$$\gamma\Delta t\mathbf{G}\Delta\mathbf{p} = \mathbf{M}^*(\mathbf{v} - \hat{\mathbf{v}}), \tag{4}$$

where $\hat{\mathbf{v}}$ is the intermediate velocity. Left multiplying both sides of (4) by ${}_\tau\mathbf{G}_\mathrm{L}\mathbf{M}^{-1}$,

$$\gamma\Delta t\,{}_\tau\mathbf{G}_\mathrm{L}\mathbf{M}^{-1}\mathbf{G}\Delta\mathbf{p} = {}_\tau\mathbf{G}\mathbf{v} - {}_\tau\mathbf{G}\hat{\mathbf{v}} + {}_\tau\mathbf{G}_\mathrm{L}\mathbf{M}^{-1}\overline{\mathbf{M}}^*(\mathbf{v} - \hat{\mathbf{v}}) \tag{5}$$

is obtained, where $\overline{\mathbf{M}}^*$ equals $\mathbf{M}^* - {}_\mathrm{L}\mathbf{M}$. If the following pressure Poisson equation (PPE)

$$\gamma\Delta t\,{}_\tau\mathbf{G}_\mathrm{L}\mathbf{M}^{-1}\mathbf{G}\Delta\mathbf{p} = -{}_\tau\mathbf{G}\hat{\mathbf{v}} \tag{6}$$

is solved, then Eq. (5) is reduced as

$${}_\tau\mathbf{G}\mathbf{v} + {}_\tau\mathbf{G}_\mathrm{L}\mathbf{M}^{-1}\overline{\mathbf{M}}^*(\mathbf{v} - \hat{\mathbf{v}}) = \mathbf{0}. \tag{7}$$

Since the linear convergence of the state variables is expected for the present definition of $\mathbf{M}^*$, $\hat{\mathbf{v}}$ agrees with $\mathbf{v}$ asymptotically in the nonlinear iterations. Therefore, the second term of (7) will vanish asymptotically, and Eq. (1b) for the unknown fluid velocity is satisfied.

It follows from the above formulation that the monolithic equation system is split into the equilibrium equations (2a) and (3) and the PPE (6), and, different from the other studies using the algebraic splitting, the Schur complement is never produced. The proposed method is summarized as follows: In the nonlinear iterations, Eq. (3) is solved to derive the intermediate velocity, Eq. (6) is solved to determine the current pressure such that the current velocity satisfies the incompressibility constraint, and Eq. (2a) is solved to derive the current velocity.

3.4 Parallel computation

The matrix–vector products provide the most expensive computations in iterative solvers. Therefore, the parallel solution procedure is employed based on the mesh decomposition as follows: The matrix–vector product is computed using a subdomain mesh at each computational node using the element–by–element method, and the nodal data on the domain interface is transferred to complete the corresponding nodal data.

4 NUMERICAL EXAMPLE

4.1 Problem Setup

Mimicking the small fly, the span length L_w and the chord length c_w of the wing are 2.5mm and 0.8mm, respectively. The material properties of air are $\rho = 1.18\times10^{-3}$g/cm^3 and the viscosity $\mu = 1.82\times10^{-4}$g/(cm s). Taking into account the surface micromachining, the following setup is used: The wing membrane is made of the polyimide (the mass density ρ = 1.43g/cm^3, the Young's modulus E = 3GPa, and the Poisson's ratio ν = 0.4), and the thickness t_w is 1–2μm. The leading edge is made of the single crystal silicon (ρ = 2.383g/cm^3, E =

180GPa, and v = 0.3), and the dimension of the cross section is 100μm (width) ×50μm (thickness). The plate spring is made of the same material of the wing membrane, and the length l_s is larger than 50μm for the bending motion.

The amplitude u_0 and the flapping frequency f_φ of the micro actuator is assumed as follows: u_0 is smaller than 100μm based on the actual micro actuator in the MEMS technology, and f_φ is from 100Hz to 1,000Hz based on the actual insects. The design objective is to find the solution that can generate the lift F_L larger than 7μN, which is the weight of the small fly.

4.2 Analysis Setup

The leading edge, the plate spring, and the wing plane are modeled using mixed interpolation of tensorial components shell elements [11] (Fig. 4A, number of nodes: 225, number of elements: 196), while the fluid domain is modeled using stabilized linear equal–order–interpolation velocity–pressure elements [10] (Figs. 4B and C, number of nodes: 46,911, number of elements: 254,352). Δt is set at $1/f_\varphi/5{,}000$. The computational environment is a multiple core processor (10 core Xeon 2.8GHz×2CPU, 32GB memory).

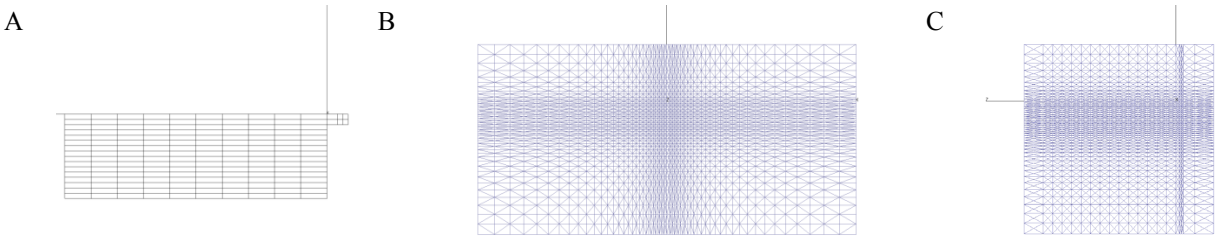

Figure 4: The present finite element meshes. A: *yz*–plane view of the shell mesh. B: *xy*–plane view of the fluid mesh. C: *yz*–plane view of the fluid mesh.

4.3 Results and discussion

In this study, the satisfactory design solutions were found from the parametric study. The dimensional parameters u_0, l_s, and t_w were set at 80μm, 50μm, and 1.6μm, respectively, and f_φ = 428Hz, which is chosen as the design and control parameter, gave the average lift larger than the weight of the small fly (7μN). The time histories of the displacement in this case were given in Fig. 5. As shown in this figure, the wing tip displacement was about 19 times larger than the wing base displacement due to the resonance. The lift variation for flapping frequency is shown in Fig. 6. As shown in this figure, the satisfactory design solutions exist from about 410 to 460Hz (DW).

5 CONCLUDING REMARKS

In this study, the FSI design of the insect–like micro flapping wing was proposed. The concept can be summarized as the FSI–cause of the pitching motion, the 2.5D–structure, and the amplification of the stroke angle using the resonance. The design problem was set taking into account the parameters of the model insect and the constraints from the MEMS technology. The projection method for the monolithic FSI equations was used for the strongly coupled FSI analysis. The existence of the DW shows the possibility of the insect–like MEMS–based MAVs.

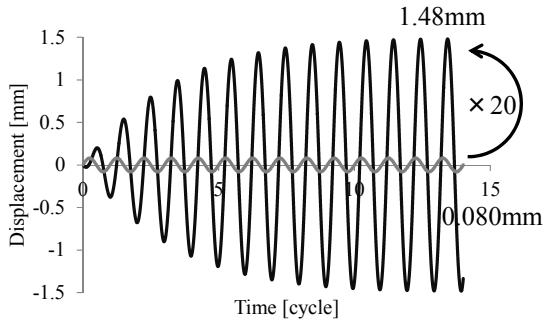

Figure 5: Time histories of the displacement. The black line indicates the wing tip displacement, while the gray line indicates the wing base displacement.

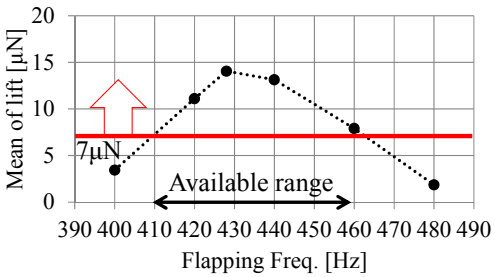

Figure 6: Area of the satisfactory design solutions in the design parameter space or the Design Window (DW).

REFERENCES

[1] Ishihara, D. and Yoshimura, S. A monolithic method for fluid–shell interaction based on consistent pressure Poisson equation. *International Journal for Numerical Methods in Engineering* (2005) **64**:167–203.

[2] Ishihara, D. and Horie, T. A projection method for the interaction of an incompressible fluid and a structure using new algebraic splitting. *Computer Modeling in Engineering & Sciences* (2014) **101**:421–440.

[3] Ishihara, D., Jeong, M.J., Yoshimura, S. and Yagawa, G. Design window search using continuous evolutionary algorithm and clustering –its application to shape optimization of microelectrostatic actuator. *Computers & Structures* (2002) **80**:2469–2481.

[4] Ishihara, D., Horie, T., Niho, T. and Baba, A. Hierarchal decomposition for the structure–fluid–electrostatic interaction in a microelectromechanical system. *Computer Modeling in Engineering & Sciences* (2015) **108**:429–452.

[5] Niho, T., Horie, T., Uefuji, J. and Ishihara, D. Stability analysis and evaluation of staggered coupled analysis methods for electromagnetic and structural coupled finite element analysis. *Computers & Structures* (2017) **178**:129–142.

[6] Ishihara, D., Horie, T. and Denda, M. A two dimensional computational study on fluid–structure interaction cause of wing pitch changes in dipteran flapping flight. *Journal of Experimental Biology* (2009) **212**:1–10.

[7] Ishihara, D., Yamashita, Y., Horie, T., Yoshida, S. and Niho, T. Passive maintenance of high angle of attack and its lift generation during flapping translation in crane fly wing. *Journal of Experimental Biology* (2009) **212**:3882–3891.

[8] Ishihara, D., Horie, T. and Niho, T. An experimental and three–dimensional computational study on the aerodynamic contribution to the passive pitching motion of flapping wings in hovering flies. *Bioinspiration & Biomimetics* (2014) **9**:046009.

[9] Ishihara, D. and Horie, T. Passive mechanism of pitch recoil in flapping insect wings. *Bioinspiration & Biomimetics* (2017) **12**:016008.

[10] Tedzduyar, T.E., Mittal, S., Ray, S.E. and Shih R. Incompressible flow computations with stabilized bilinear and linear equal–order–interpolation velocity–pressure elements. *Computer Methods in Appled Mechanics & Engineering* (1992) **95**:221–242.

[11] Noguchi, H. and Hisada, T. Sensitive analysis in post–buckling problems of shell structures. *Computers & Structures* (1993) **47**: 699–710.